Ann. Rev. Biophys. Bioeng. 1984. 13 : 247–68

TOTAL INTERNAL REFLECTION FLUORESCENCE

Daniel Axelrod

Biophysics Research Division and Department of Physics, University of Michigan, Ann Arbor, Michigan 48109

Thomas P. Burghardt

Cardiovascular Research Institute, University of California, San Francisco, California 94143

Nancy L. Thompson

Department of Chemistry, Stanford University, Stanford, California 94305

INTRODUCTION

Total internal reflection fluorescence (TIRF) is an optical effect particularly well-suited to the study of molecular and cellular phenomena at liquid/solid interfaces. Such interfaces are central to a wide range of biochemical and biophysical processes: binding to and triggering of cells by hormones, neurotransmitters, and antigens; blood coagulation at foreign surfaces; electron transport in the mitochondrial membrane; adherence and mobility of bacteria, algae, and cultured animal cells to surfaces; and possible enhancement of reaction rates with cell surface receptors upon nonspecific adsorption and surface diffusion of an agonist. Liquid/solid interfaces also have important medical and industrial applications: e.g. detection of serum antibodies by surface immobilized antigens; and the manufacture of biochemical products by surface-immobilized enzymes.

Total internal reflection spectroscopy for optical absorption studies (called attenuated total reflection or ATR) was developed somewhat earlier than the fluorescence applications and has been widely used in surface chemistry studies (17). The basic book in this area is *Internal Reflection*

0084–6589/84/0615-0247$02.00

Spectroscopy by Harrick (18). Total internal
combined with Raman spectroscopy (24, 32), X-ray fluorescence (2), infrared absorption spectroscopy (16), and light scattering (3, 33).

As a technique for selective surface illumination, total internal reflection fluorescence was first introduced by Hirschfeld (21) for solid/liquid interfaces, Tweet et al (39) for liquid/air interfaces, and Carniglia & Mandel (13) for high refractive index liquid/solid interfaces. TIRF has been combined with a variety of other conventional fluorescence techniques (polarization, Förster energy transfer, microscopy, spectral analysis, photobleaching recovery, and correlation spectroscopy) for a variety of purposes (detection of molecular adsorption; measurement of adsorption equilibrium constants, kinetic rates, surface diffusion, adsorbate conformation; and observation of cell/substrate contact regions). This review is organized according to those purposes. We begin with a summary of the relevant optical theory.

THEORY

Evanescent Intensity

When a light beam propagating through a transparent medium of high index of refraction (e.g. a solid glass prism) encounters an interface with a medium of a lower index of refraction (e.g. an aqueous solution), it undergoes total internal reflection for incidence angles (measured from the normal to the interface) greater than the "critical angle." The critical angle θ_c, is given by

$$\theta_c = \sin^{-1}(n_2/n_1), \qquad 1.$$

where n_2 and n_1 are the refractive indices of the liquid and the solid, respectively. Although the incident light beam totally internally reflects at the interface, an electromagnetic field called the "evanescent wave" penetrates a small distance into the liquid medium and propagates parallel to the surface in the plane of incidence. The evanescent wave is capable of exciting fluorescent molecules that might be present near the interface. This effect has been regarded as experimental proof of the existence of the evanescent wave (44).

The evanescent electric field intensity $I(z)$ decays exponentially with perpendicular distance z from the interface:

$$I(z) = I_0 e^{-z/d},$$

where

$$d = \frac{\lambda_0}{4\pi}[n_1^2 \sin^2\theta - n_2^2]^{-1/2} \qquad 2.$$

for angles of incidence $\theta > \theta_c$ and light wavelength in vacuum λ_0. Depth d is independent of the polarization of the incident light and decreases with increasing θ. Except for $\theta \simeq \theta_c$ (where $d \to \infty$), d is on the order of λ_0 or smaller.

The intensity at $z = 0$, I_0, depends on both the incidence angle θ and the incident beam polarization. I_0 is proportional to the square of the amplitude of the evanescent electric field $\mathbf{E}$ at $z = 0$.[1] (These expressions are given in the next subsection.) For incident electric field intensities $\mathcal{I}^{\parallel,\perp}$ with polarizations parallel and perpendicular, respectively, to the plane of incidence, the evanescent intensities $I_0^{\parallel,\perp}$ are

$$I_0^{\parallel} = \mathcal{I}^{\parallel} \cdot \frac{4 \cos^2 \theta (2 \sin^2 \theta - n^2)}{n^4 \cos^2 \theta + \sin^2 \theta - n^2} \qquad 3.$$

and

$$I_0^{\perp} = \mathcal{I}^{\perp} \cdot \frac{4 \cos^2 \theta}{1 - n^2}, \qquad 4.$$

where

$$n = n_2/n_1 < 1. \qquad 5.$$

Figure 1 illustrates $I_0^{\parallel,\perp}$ as functions of θ. Note several features: (*a*) the evanescent intensity $I_0^{\parallel,\perp}$ is not weak and can be several times stronger than the incident intensity for angles of incidence within a few degrees of the critical angle; (*b*) the intensities of the two polarizations are different, with $I_0^{\parallel}$ somewhat more intense for all θ; (*c*) $I_0^{\parallel,\perp}$ both approach zero as $\theta \to 90°$.

Evanescent Fields

The phase behavior of the $\mathbf{E}$ field is quite remarkable (7). The field components are listed below, with incident electric field amplitudes $A^{\parallel,\perp}$ and phase factors relative to those of the incident $\mathbf{E}$ and $\mathbf{H}$ fields' phase at $z = 0$. (The coordinate system is chosen such that the x–z plane is the plane of incidence.)

$$E_x = \left[\frac{2 \cos \theta \, (\sin^2 \theta - n^2)^{1/2}}{(n^4 \cos^2 \theta + \sin^2 \theta - n^2)^{1/2}} \right] A_{\parallel} e^{-i(\delta_{\parallel} + \pi/2)}, \qquad 6.$$

$$E_y = \left[\frac{2 \cos \theta}{(1 - n^2)^{1/2}} \right] A_{\perp} e^{-i\delta_{\perp}}, \qquad 7.$$

[1] The evanescent intensity that excites fluorescence is given by $|\mathbf{E}|^2$ (12, 13). Generally, the energy flux of an electromagnetic field is given by the real part of the Poynting vector, $\mathbf{S} = (c/4\pi)\mathbf{E} \times \mathbf{H}$, where $\mathbf{H}$ is the magnetic field. For a transverse field, $|\mathbf{S}|$ is proportional to $|\mathbf{E}|^2$. Note that for an evanescent wave, $|\mathbf{S}|$ is not proportional to $|\mathbf{E}|^2$.

$$E_z = \left[\frac{2\cos\theta\sin\theta}{(n^4\cos^2\theta+\sin^2\theta-n^2)^{1/2}}\right]A_{\|}e^{-i\delta_{\|}}, \quad 8.$$

where

$$\delta_{\|} \equiv \tan^{-1}\left[\frac{(\sin^2\theta-n^2)^{1/2}}{n^2\cos\theta}\right] \quad 9.$$

and

$$\delta_{\perp} \equiv \tan^{-1}\left[\frac{(\sin^2\theta-n^2)^{1/2}}{\cos\theta}\right]. \quad 10.$$

Note that the evanescent electric field is transverse to the propagation direction $(+x)$ only for the $\perp$ polarization. The $\|$ polarization **E** field

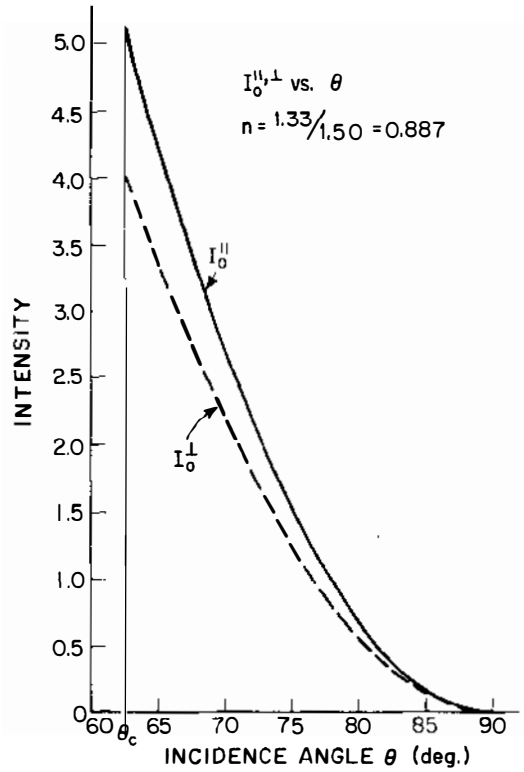

Figure 1 Intensities $I_0^{\|,\perp}$ vs incidence angle θ, for $n = 0.887$, corresponding to a critical angle of $\theta_c = 62.46°$. Intensity is expressed as the ratio of evanescent intensity at $z = 0$ to the incident intensity for each polarization.

"cartwheels" along the surface with a spatial period of $\lambda_0/(n_1 \sin \theta)$ as shown schematically in Figure 2.

For absorbers with magnetic dipole transitions, the evanescent magnetic field **H** is relevant. Assuming equal magnetic permeabilities at both sides of the interface, the components of the evanescent field **H** at $z = 0$ are

$$H_x = \left[\frac{2 \cos \theta \, (\sin^2 \theta - n^2)^{1/2}}{(1-n^2)^{1/2}}\right] A_\perp e^{-i(\delta_\perp - \pi)}, \quad 11.$$

$$H_y = \left[\frac{2n^2 \cos \theta}{(n^4 \cos^2 \theta + \sin^2 \theta - n^2)^{1/2}}\right] A_\parallel e^{-i(\delta_\parallel - \pi/2)}, \quad 12.$$

$$H_z = \left[\frac{2 \cos \theta \sin \theta}{(1-n^2)^{1/2}}\right] A_\perp e^{-i\delta_\perp}. \quad 13.$$

The angular dependence of the phase factors $\delta_\perp$ and $\delta_\parallel$ gives rise to a measurable longitudinal shift of a finite-sized incident beam, known as the Goos-Hanchen shift (29). Viewed physically, some of the energy of a finite-width beam crosses the interface into the lower refractive index material, skims along the surface for a Goos-Hanchen shift distance ranging from a fraction of a wavelength (at $\theta = 90°$) to infinite (at $\theta = \theta_c$), and then reenters the higher refractive index material.

In many TIRF experiments, an incident laser beam of Gaussian intensity profile passes through a converging lens, enters the side of a prism, and then focuses at a totally reflecting surface. The nature of the evanescent

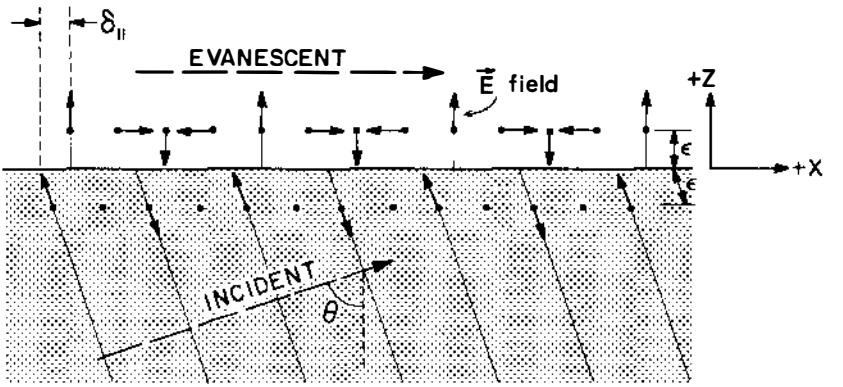

Figure 2 Electric field vectors of incident and evanescent light for the ∥ incident polarization, showing the phase lag $\delta_\parallel$ and the "cartwheel" or elliptical polarization of the evanescent field in the plane of propagation. Both the incident and evanescent vectors refer to the $z = 0$ position; they are schematically displaced a distance ε ($\rightarrow 0$) below and above the interface along their constant phase lines for pictorial clarity only.

illumination produced by such a focused finite beam geometry has been investigated in general (12). For typical experimental conditions, the evanescent illumination is of an elliptical Gaussian profile and the polarization and penetration depth are approximately equal to those of a plane wave.

The angular distribution of evanescent wave-excited fluorescence when viewed through the prism is anisotropic. A complete discussion appears in Lee et al (26).

Intermediate Layers

Thus far, the theoretical discussion has assumed that the medium in which the evanescent wave propagates contains no light absorbers, light scatterers, layers of unmatched refractive index, or electrical conductors. The effect of such intermediate layers is clearly relevant to TIRF.

The presence of absorbers perturbs the evenescent wave and thereby disturbs the linearity between actual surface concentration of absorber and observed fluorescence. (This effect is roughly analogous to the "inner filter" effect in conventional fluorimetry in which a high concentration of fluorophore attenuates the incident light.) Burghardt & Axelrod (10) have calculated the magnitude of this nonlinear effect as a function of surface concentration of absorbing material of arbitrary thickness. The result of this calculation shows that typical TIRF experiments are well within the linear range in which observed fluorescence and surface concentration are proportional. Harrick (18) displays results of an analogous calculation of the effect of absorbers on the intensity of the reflected laser beam.

Aside from the effect of absorbers, the presence of an intermediate layer of a homogeneous dielectric material of unmatched refractive index deposited on the totally reflecting surface can clearly affect the evanescent wave intensity and characteristic decay distance (31). Total internal reflection may even occur at the interface between the intermediate layer and the low refractive index medium. Regardless of their refractive indices, intermediate layers cannot thwart total internal reflection at some interface in the system if it would have occurred without the intermediate layers.

If a metallic conductor is deposited onto the interface, entirely new phenomena can be observed (15, 42). Rather than emitting fluorescence isotropically, an evanescent wave-excited dye molecule adsorbed to the intermediate metal layer will tend to transfer its energy to surface plasmons in the adjacent metal. If the metal film is sufficiently thin, the emission can then be observed as a hollow cone of light propagating back through the prism. If a semiconductor thin film is deposited on the interface, one might observe charge transfer between an excited dye molecule and the conduction band of the semiconductor (30).

The scattering of evanescent light by an intermediate layer has been treated theoretically (14). Evanescent light scattering is the basis of the dark field microscope introduced by Ambrose (3) for examining cultured biological cell-substrate contacts and also is the basis of a study of photoreceptor membrane attached to optical fibers (33). Whether scattering significantly increases the effective depth of light penetration into the low optical density medium has been tested in some of the experimental systems discussed in following sections.

In the next three sections, we review experimental results with TIRF optics.

ADSORPTION AT EQUILIBRIUM: DETECTION AND CALIBRATION

In an early published application of TIRF, Tweet et al (39) measured the emission spectrum and quenching behavior of chlorophyll *a* monolayers at an aqueous/air interface (see Figure 3*a*). TIRF provided a means of detecting the weak fluorescence from a very dilute monolayer with a high degree of exclusion of direct and scattered mercury arc excitation light.

A short note by Hirschfeld (21) introduced TIRF at a solid/liquid interface. A special cell (Figure 3*b*) designed to fit a commercial absorption spectrophotometer and providing for multiple total reflections of excitation light in a fused silica microscope slide was used to study the fluorescence of fluorescein in the 1–1000 ppm bulk concentration range. The goal here was to study bulk-dissolved dye in the vicinity of an interface rather than adsorbed dye. Hirschfeld lists several advantages of TIRF over conventional illumination for this purpose. (*a*) The small depth of penetration of the evanescent wave combined with observation of fluorescence emitted back into the prism could allow studies of turbid or highly adsorbing solutions. (*b*) The intensity/concentration relationship was linear at up to two orders of magnitude higher concentration for TIRF than for conventional illumination. (*c*) Effects of adsorption or the proximity of glass upon the fluorescence properties could be detected by changing the excitation incidence angle and thereby the penetration depth. (*d*) The possibility of multiple total reflections in the same prism allows the excitation to interact with the sample many times, thereby increasing sensitivity. (*e*) Many fluorescent materials (dyes, labeled proteins, etc) strongly adsorb onto solid surface from very dilute solutions, often unavoidably depleting the bulk concentration of the fluorophore and dramatically increasing the effective local concentration of the fluorophore in the proximity of the surface. Selective surface excitation by TIRF thereby leads to an effective enhancement of sensitivity to extremely low concentrations of fluorophore.

The sensitivity of TIRF to adsorbed films containing a fluorophore can be upgraded further, as described by Harrick & Loeb (19, 20). With a prism in which multiple total internal reflection of excitation light takes place and also in which much of the fluorescence emission is also trapped by total internal reflection, a large fluorophore-coated surface area can be observed with a large effective solid angle of light collection (Figure 3*c*). In one application of this sort of optics, a film of dansyl-labeled bovine serum albumin (BSA) was adsorbed onto a fused silica prism and dried in air. Note that the fluorescence here is not excited by the evanescent wave as

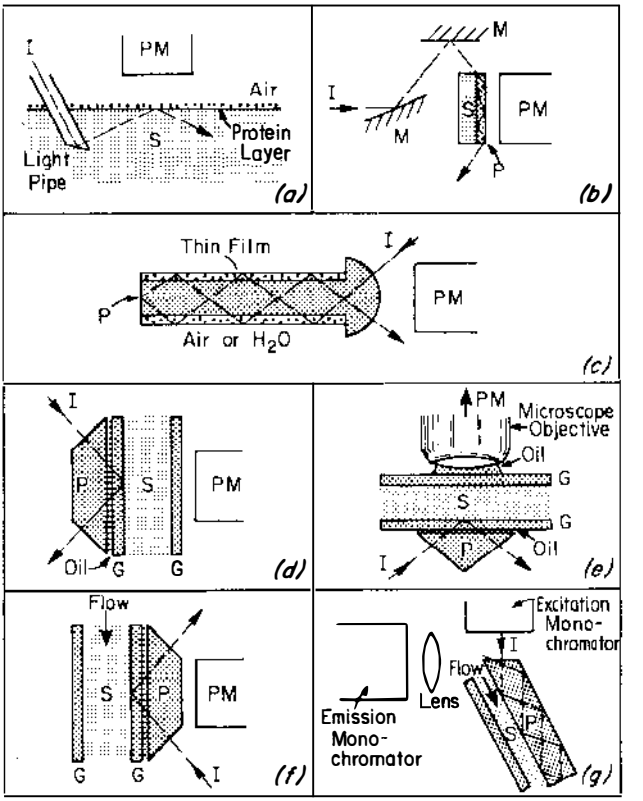

Figure 3 Optical designs for some TIRF experiments as described in the text. These are simplified drawings showing the general excitation geometries with most of the lenses in the excitation and emission pathways not shown. The following abbreviations are used: G, glass microscope slide; PM, photomultiplier (always assumed to be preceded by a colored optical filter to block scattered excitation light); P, prism (usually optical glass or fused silica); S, solution containing fluorophore (usually a fluorescence-labeled serum protein); M, mirror; I, incident light beam.

previously described, since total internal reflection occurs at the protein film/air interface instead of the silica prism/film interface. Rather, TIR serves to confine both the excitation and emission light on the film-coated prism, allowing entrance and exit of light only at one hemicylindrically shaped end.

Kronick & Little (25) have employed TIRF with an immunologically specific antigen-coated surface to assay for specific fluorescent-labeled antibodies in solution. The antigen complimentary to the antibody is conjugated to egg albumin and then is physically adsorbed onto a fused silica slide. The excitation light, from a helium cadmium laser, is introduced into the slide via an optical coupling with a trapezoidal shaped prism (Figure 3*d*). As fluorescent antibodies attach to the surface-immobilized antigens, the evanescent wave-excited fluorescence increases. The chief limit to the specific sensitivity of this assay is the nonspecific binding of antibodies to the egg albumin coated surface. This problem is less severe with strongly binding antigen-antibody combinations and specially treated surfaces that reduce nonspecific protein binding. With a silica slide coated by the antigen morphine, a concentration of 2×10^{-7} M of dissolved fluorescent labeled antimorphine could be detected specifically in their TIRF system. The system remains to be tested for success in assaying antibodies in blood serum.

A very elegant TIRF method and apparatus for assaying for viruses in human blood serum (called a "virometer") has been described by Hirschfeld and co-workers (22, 23) for use on the stage of an upright microscope (Figure 3*e*). A serum sample, mechanically filtered to eliminate particulates larger than virus particles, is treated with a nucleic-acid binding fluorophore and then observed by TIRF. As fluorescent-labeled constituents in the serum enter and leave the evanescent wave in the bulk, they cause visible fluorescence fluctuations. Because of their large size, the virions diffuse by Brownian motion more slowly than other fluorescent constituents and thereby cause slower fluorescence fluctuations. By autocorrelating the fluctuations, this slower component can be resolved. From the relative amplitude of this slow component, the absolute concentration of virions can be calculated. Mixtures of two fluorescent nucleic acid stains of widely different emission spectra could allow distinction between different types of virions. TIRF illumination, as opposed to conventional microscope epi-illumination, served mainly to (*a*) define a very small distance—the penetration depth d—through which virions can traverse in a short time, and (*b*) avoid background fluorescence from out-of-focus planes in the solution. The principles of the virometer are similar to some of those later applied in total internal reflection/fluorescence correlation spectroscopy (TIR/FCS) (38) for other purposes to be described later in the next section.

In TIRF experiments in which an adsorbed fluorophore is in reversible chemical equilibrium with bulk-dissolved fluorophore, it is desirable to determine what proportion of the observed fluorescence arises from actually adsorbed fluorophore versus bulk fluorophore merely close enough to the surface to be excited by the evanescent wave or scattered incident light. Given either (*a*) an independent calibration of adsorbed surface concentration (10), (*b*) an independent measurement of the total number of illuminated fluorescent molecules (36), or (*c*) an independent measurement of fluorescence from a nonadsorbant in a TIRF apparatus (27, 32a), the proportion of adsorbed vs bulk molecules can be calculated. Alternatively, the fraction of illuminated fluorophore that is adsorbed can be determined from the abscissa intercept of a plot of evanescent field depth (which can be varied with incidence angle; see Equation 2) vs measured fluorescence (corrected for the variation in evanescent intensity with incidence angle; see Figure 1). Another method of determining the adsorbed fraction of illuminated fluorophore is to interpolate the degree of polarization anisotropy of the sample's fluorescence (with adsorbed and bulk fluorophore in equilibrium) between that of purely adsorbed and purely solubilized fluorophore. (This method assumes slower rotational motion of adsorbed fluorophore compared to solubilized fluorophore.) Finally, the ratio r of fluorescent intensity to the intensity of the water solvent's Raman scattering peak can be compared between a surface under evanescent illumination and a bulk solution under conventional illumination. The relative values of ratio r are directly related to the fraction of illuminated fluorophore that is adsorbed. A large increase in ratio r (typically observed upon serum protein adsorption) demonstrates the dominance of surface adsorbed to bulk-dissolved fluorophore under TIRF illumination.

CHEMICAL KINETICS AND SURFACE DIFFUSION

It is often of interest to know how rapidly a solute adsorbs to a surface, how long it stays there before it desorbs, and whether it diffuses along the surface while adsorbed. Many of the studies in this area involve adsorption of blood serum proteins to nonbiological surfaces, partly because of the relevance to blood coagulation in medical prostheses.

The most direct approach to chemical kinetics in a TIRF system is a "concentration-jump": rapidly increasing bulk concentration from zero to a final value to measure adsorption rates, or the reverse to measure desorption rates. Employing this approach, Watkins & Robertson (41) measured the time course of uptake (as well as equilibrium adsorption isotherms) for fluorescein-labeled albumin, γ-globulin, and fibrinogen onto

Siliclad or silicone rubber-coated surfaces from static solution, and for γ-globulin onto silicone rubber from flowing solutions (Figure 3*f*). One qualitatively significant finding was a reversibly bound layer of γ-globulin constituting as much as 40% of the total surface bound protein.

Lok et al (27, 28) continued these type of studies with bovine albumin and fibrinogen adsorbing onto silicone rubber from flowing solutions. They find that the initial rate of adsorption for both proteins is diffusion limited (i.e. every solute molecule hitting an available site on surface sticks to it), and also that fibrinogen uptake does not plateau after several hours and may adsorb in multilayers. A particularly careful discussion of contributions from bulk-dissolved fluorophore and scattered incident light arising in artificial polymer coatings is presented in Lok et al (27).

The possibility exists that extrinsic fluorophores on serum proteins might affect the rates and amounts of physical adsorption. To avoid this possibility, Van Wagenen et al (40) studied the intrinsic tryptophan fluorescence of bovine serum albumin and γ-globulins adsorbed to fused silica following concentration jumps in a flushable cell. The general optical arrangement for TIRF was similar to that of Watkins & Robertson (41) (Figure 3*f*), but with the variations that the light source was an Hg-Xe arc instead of an argon laser and that both the excitation and emission wavelengths could be scanned by monochromators in order to obtain spectra. Both proteins studied exhibited a very rapid initial phase of adsorption from low bulk concentrations; γ-globulin also showed a prolonged slow uptake component continuing for at least 40 min after its introduction. Albumin adsorption continued to occur at concentrations exceeding those required for monolayer coverage, leading to the authors' inference of multilayers on the surface. No evidence is available as yet as to whether extrinsic probes affect the adsorption behavior seen with probe-free serum proteins.

Beissinger & Leonard (6) employed a multiple internal reflection prism adaptable to a commercial spectrofluorimeter to measure the concentration jump adsorption kinetics of fluorescein-labeled human γ-globulin to fused silica under flow conditions (Figure 3*g*). Again, both reversible and relatively irreversible binding was detected, with the reversible component increasing linearly with bulk concentration. Adsorption rates were found to be proportional to solution concentration.

Surface desorption rates and surface diffusion coefficients can be observed without perturbing the chemical equilibrium (as occurs in a concentration jump) by combining TIR with either fluorescence photobleaching recovery (TIR/FPR) or fluorescence correlation spectroscopy (TIR/FCS) (38). In TIR/FPR, adsorbed molecules are irreversibly photobleached by a flash of laser beam focused at a total internal reflection

surface; subsequent fluorescence recovery vs time is monitored by an attentuated evanescent intensity as bleached molecules exchanged with unbleached ones from the solution or from surrounding nonilluminated regions of the surface (Figure 4). In TIR/FCS, the evanescent intensity is maintained at a constant and fairly dim level throughout, and spontaneous fluorescence fluctuations due to individual molecules entering and leaving a well-defined portion of the evanescent field are electronically autocorrelated. In general, the shape of the theoretical TIR/FPR and TIR/FCS curves depends in a complex manner upon the bulk and surface diffusion coefficients, the size of the illuminated or observed region, and the adsorption and desorption kinetic rates. However, under appropriate experimental conditions, the rate constants and surface diffusion coefficients can be readily obtained.

When the surface residency time of a reversibly bound adsorbant is much longer than the time necessary to enter or leave the vicinity of the observed surface area, the process is in the "reaction limit." Mathematically, this limit is described by

$$\frac{\beta}{k_2} \gg \frac{(\bar{C}/\bar{A})^2}{D_A} \qquad 14.$$

Surface residency time $\gg$ Bulk diffusion time

where

$$\beta = \begin{cases} 1 \text{ (for TIR/FPR), or} \\ \text{fraction of surface binding sites that are unoccupied} \\ \text{at equilibrium (for TIR/FCS),} \end{cases}$$

$\bar{A}$ = equilibrium concentration of bulk solute,

$\bar{C}$ = equilibrium concentration of surface adsorbed solute,

D_A = diffusion coefficient of solute in the bulk.

In the reaction limit for a large illuminated or observed area, the fluorescence recovery (for TIR/FPR) and the autocorrelation function (for TIR/FCS) depend only on k_2 and the shape is exponential. Thus, in the reaction limit the desorption rate k_2 can be obtained easily. Increasing the bulk concentration $\bar{A}$ or reducing the size of the observation area tends to drive the process toward the reaction limit.

If the opposite relationship to that of Equation 14 holds, for a large illuminated or observed area, the process is in the "bulk diffusion limit," in which TIR/FPR and TIR/FCS curves depend only on D_A and the equilibrium concentrations. Physically, this limit occurs when the surface behaves as a nearly perfect sink with respect to the adsorbing molecules.

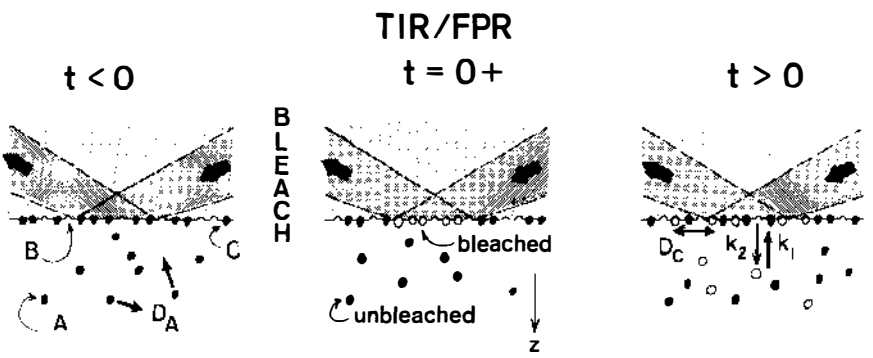

Figure 4 Exchange of surface-adsorbed bleached molecules with unbleached ones in TIR/FPR experiment. Symbols are as follows: A, unbleached solute molecules in the bulk solution, denoted by filled circles; B, unoccupied surface binding sites, denoted by hemicircular indentations in the surface; C, unbleached adsorbed molecules, which in the region of evanescent illumination, give rise to fluorescence; D_A and D_C, bulk and surface diffusion coefficients, respectively; k_1 and k_2, the adsorption and desorption kinetic rates, respectively. Bleached molecules, whether in the bulk solution or on the surface, are denoted by open circles.

Between the reaction and the bulk diffusion limits, the curves depend on both k_2 and D_A, $\bar{A}$, and $\bar{C}$. The shape of a TIR/FPR or TIR/FCS curve can thus distinguish between reaction limited, bulk diffusion limited, and intermediate processes. Thompson et al (38) provide a mathematical and physical description of these limits and intermediate cases; Thompson & Burghardt (37) further develop the meaning of these limits in terms of a microscopic model of reactions with target sites in one, two, or three dimensions.

If surface diffusion exists, its characteristic time clearly depends upon the size of the area across which an adsorbed molecule diffuses. Surface diffusion can thereby be distinguished from the adsorption/desorption process simply by changing the size of the illuminated region (for TIR/FPR) or observed region (for TIR/FCS). If surface diffusion occurs at a measurable rate, decreasing the illuminated or observed region size will increase the rapidity of fluorescence recovery or the autocorrelation function decay (38).

Both TIR/FPR and TIR/FCS have been confirmed as experimentally feasible (Figure 5). Using TIR/FPR, Burghardt & Axelrod (10) have measured a range of residency times of rhodamine-labeled BSA adsorbed to fused silica ranging from approximately 5 sec to at least several hours. The most "loosely" bound BSA molecules also appeared to surface diffuse with a coefficient of 5×10^{-9} cm^2/sec, fast enough to carry a BSA molecule several microns on the surface before desorption. This observation of

surface diffusion of a biological molecule may be significant in view of the hypothesis of Adam & Delbruck (1) that nonspecific adsorption and diffusion on cell surfaces might enhance agonist/receptor reaction rates.

Using TIR/FCS, Thompson & Axelrod (36) have measured the nonspecific adsorption/desorption kinetics of rhodamine-labeled immunoglobulin and insulin on serum albumin coated fused silica. Rapidly reversible adsorption could be visualized under TIR as twinkling speckles of fluorescence as molecules enter and leave the evanescent wave region. Upon on-line autocorrelation of these fluorescence fluctuations, a range of desorption times was noted, with the shortest time less than 5 ms, limited by the rate of bulk diffusion. Antibody molecules appeared to bind specifically to antigen-coated fused silica, but this was accompanied by a large amount of reversible nonspecific binding. Such nonspecific binding is difficult to avoid and perhaps occurs on cell surfaces where it may be biochemically functional via the Adam & Delbruck (1) mechanism mentioned above. In suitable systems where nonspecific binding is low, TIR/FCS and TIR/FPR should prove useful for measuring specific solute-surface kinetic rates. In

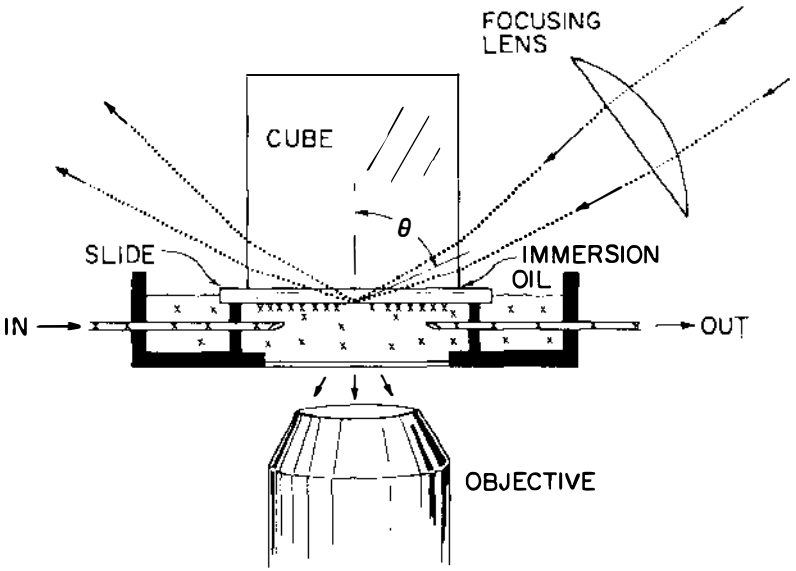

Figure 5 Experimental apparatus for TIR/FPR, for use on the stage of an inverted microscope. Fluorescent solute molecules are indicated by x's. The cubical prism and slide are made of fused silica. The drilled hole in the bottom of the dish is covered with a glass coverslip and sealed in with encapsulating resin. The apparatus for TIR/FCS is qualitatively similar, except that the inflow and outflow tubes are omitted and the spacing between the slide and the bottom coverslip is reduced to only 0.06 mm with a thin Teflon spacer to enable use of high aperture, short working distance oil immersion objectives.

principle, TIR/FCS can even measure specific solute/surface kinetic rates at equilibrium of nonfluorescent molecules by competing them with fluorescent analogs (35). In any case, TIR/FCS and TIR/FPR can be distinguished from the TIR concentration jump method by their ability to measure very rapid rates without necessitating macroscopic perturbation of the equilibrium.

MOLECULAR CONFORMATION OF ADSORBATES

The conformational and dynamical properties of adsorbed proteins can be studied by combining TIRF with conventional fluorescence spectroscopic techniques such as singlet-singlet (Förster) energy transfer and fluorescence polarization. For this purpose, a TIRF chamber easily fitted into a commercial spectrofluorimeter for spectra analysis has been designed (11) (Figure 6). Using this chamber, the authors observed a decrease in effective energy transfer rate upon adsorption in BSA multiply-labeled with the fluorophore donor/acceptor pairs of dansyl/eosin or 4-chloro-7-nitro-2,1,3-benzoxadiazole (NBD)/rhodamine. Under certain assumptions, this energy transfer change can be interpreted as a conformational change of BSA upon adsorption. The intrinsic tryptophan fluorescence of unlabeled BSA was also found to be less quenchable by iodide ion when adsorbed to fused silica than when dissolved in bulk (D. Axelrod, unpublished observation). This result indicates either a conformational change upon adsorption or reduced accessibility of iodide to tryptophan residues because of the proximity of the surface.

Using the same TIRF spectrofluorimeter chamber to measure steady state fluorescence polarization, Burghardt (8) has inferred a decreased rotational diffusion coefficient of NBD, rhodamine, or eosin fluorophores around their single covalent bonds binding them to BSA upon adsorption of the BSA to fused silica. The restricted rotational motion of the probe can be attributed to direct steric interference by the surface or to steric interference arising from a conformational change in BSA. (The same paper also contains a mathematical derivation of the expected fluorescence polarization anisotropy decay of a rotationally diffusing fluorophore while connected to an anisotropically rotationally diffusing protein.)

Preliminary experiments have been performed using TIRF with time-resolved fluorescence lifetime and anisotropy decay measurements to detect the fluorescence lifetimes and rotational motion of labeled protein at the solid/liquid interface (T. P. Burghardt and P. M. Torgerson, unpublished observations). These particular experiments utilize the unique polarization characteristics of the evanescent electric field to deduce the order of arrangement of labeled proteins in a biological structure (9).

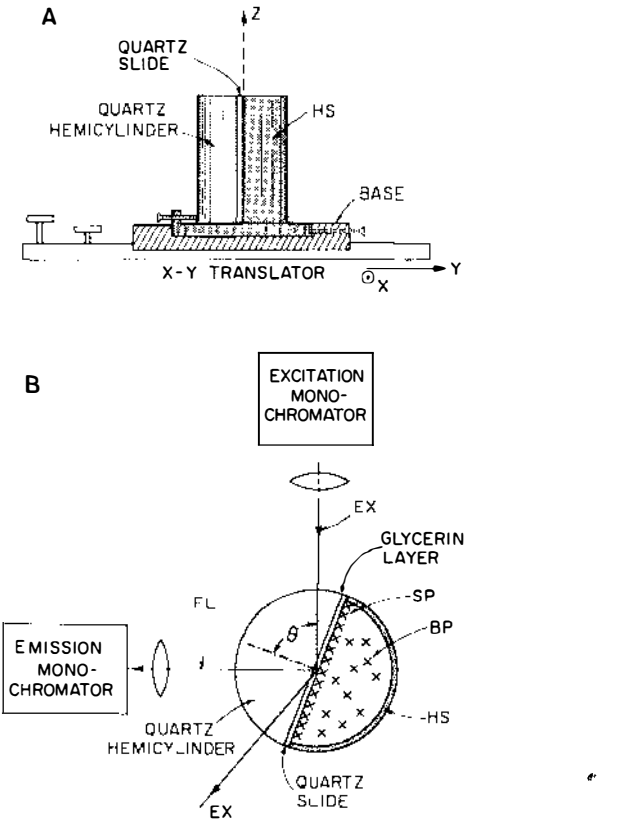

Figure 6 Two views of the total internal reflection fluorescence spectroscopy apparatus. (*A*) Side view shows the axis of rotation, *z*, about which the prism and slide and Plexiglass hemicylinder shell (HS) unit is rotated in the base to adjust the angle of incidence of the excitation light. The base is removably mounted on an *x-y* translator for lateral positioning of the unit. The apparatus fits inside the sample chamber of a commercial fluorescence spectrofluorometer. (*B*) Vertical view of the device shows the path of the excitation (EX) and the fluorescent emission (FL) through the quartz hemicylinder. Surface-adsorbed protein (SP) is illuminated by the evanescent field while in chemical equilibrium with the bulk-dissolved protein (BP). The fused silica hemicylinder has a radius of 1.3 cm and a height of 2.5 cm.

CELL/SUBSTRATE CONTACTS

TIRF can be used to excite fluorescence exclusively from regions of contact between living cultured cells and the substrate (usually plastic or glass) upon which they grow. These regions of contact are of considerable interest: they are anchors for cell motility, loci for aggregation of specific membrane proteins, and convergence points for cytoskeletal filaments. A recent review of TIRF microscopy has appeared (5).

Several experimental designs for TIRF microscopy are possible. Figure 7 (from 4) shows a design appropriate for an inverted fluorescence microscope. Phase contrast transmitted illumination and epi-illumination (i.e. through the objective) are easily interchanged with TIRF without changing the basic configuration (Figure 8). By varying the incidence angle of the totally reflecting laser beam, and thus the depth of evanescent illumination, details of the topography of the cell surface near the substrate can be revealed (4, 5).

Another TIRF design (Figure 9) (D. Axelrod, unpublished), used in an upright microscope, is particularly convenient for directly viewing cells growing in disposable plastic tissue culture dishes and works quite well despite the autofluorescence of tissue culture polystyrene plastic. (Corning brand dishes have significantly less autofluorescence than Falcon, Lux, or Nunc brands and are thereby more suitable.) Both this design and the one shown in Figure 7 permit the cells to be moved laterally while retaining TIR illumination centered in the microscope's field of view.

A third design (43) (for an inverted microscope) employs a triangular prism to guide a laser beam into a microscope slide where it undergoes multiple internal reflections (Figure 10). The cells may reside on top of the slide (for any kind of cells) (A. Brian and N. L. Thompson, unpublished) or underneath the slide (for tightly adhering cells). A novel feature is the use of intersecting laser beams (split from the same laser) at the total internal reflection surface to create a parallel line interference fringe pattern. This interference pattern can be seen on the fluorescing regions of cell/substrate contact, thereby confirming that the primary source of excitation is indeed the evanescent wave rather than light randomly scattered from the evanescent wave by the cells. Another potential application of these TIRF

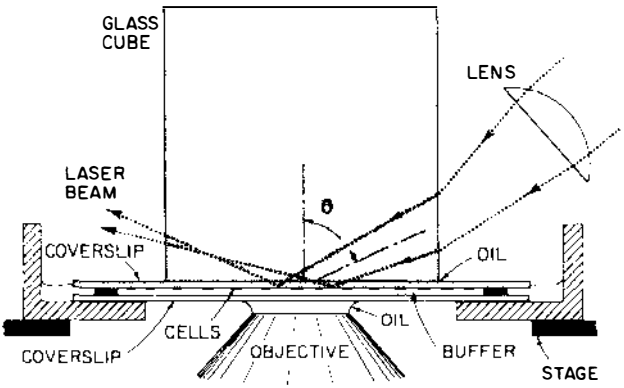

Figure 7 TIRF inverted microscope apparatus for viewing cells in culture. Cells are plated and grown on a standard glass coverslip, which is then inverted and placed in optical contact with the cubical prism via a layer of immersion oil or glycerin.

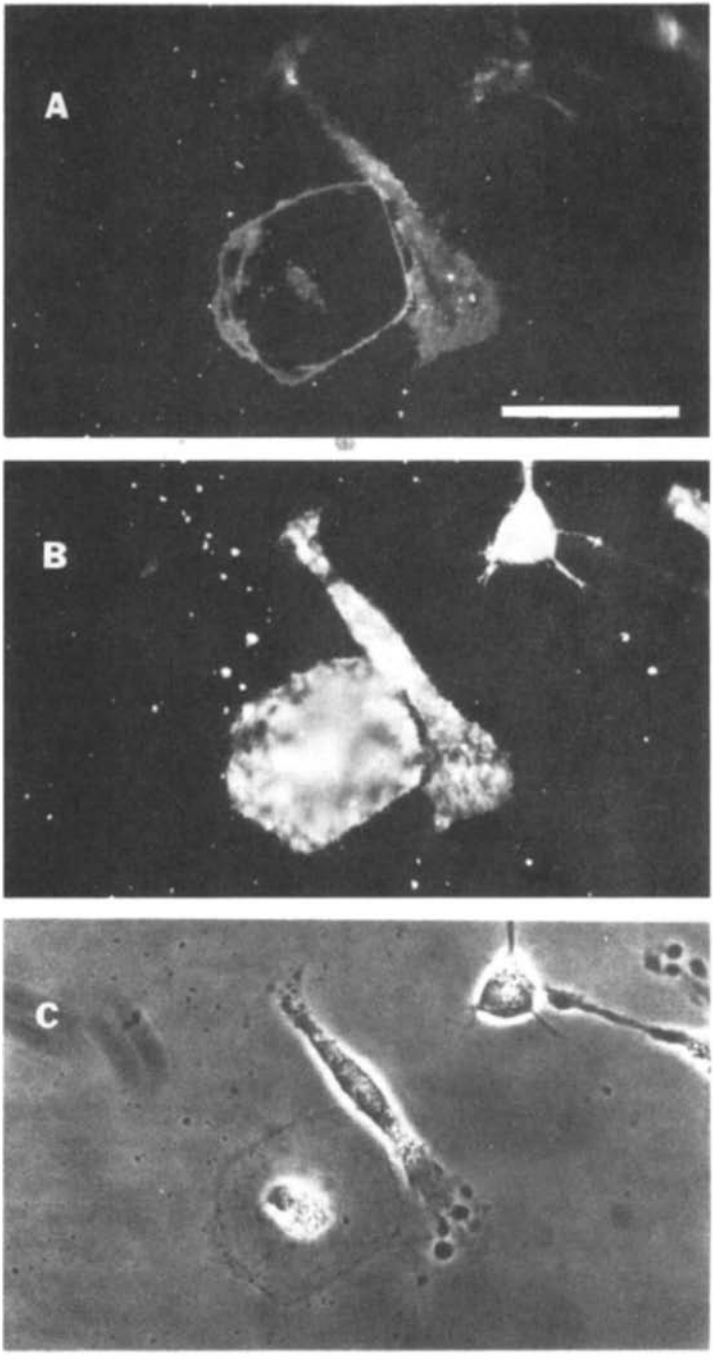

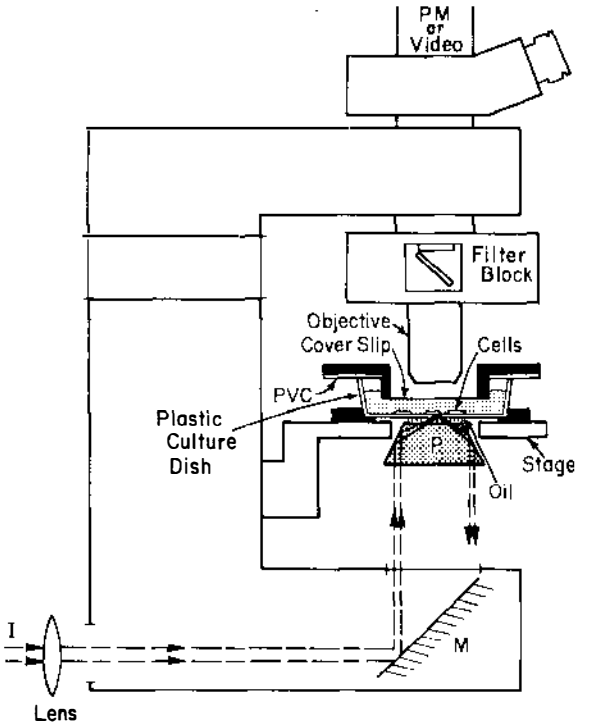

Figure 9 TIRF adapted to an upright microscope, for viewing cells in a plastic tissue culture dish. The prism is a truncated equilateral triangle. The region of the sample chamber is shown enlarged relative to the rest of the microscope for pictorial clarity. Abbreviations are as follows: I, incident light; M, mirror (part of microscope base); P, prism; PM, photomultiplier; PVC, polyvinylidene chloride ("Saran" film used to seal in a 10% CO_2 atmosphere over the tissue culture medium).

fringes is to measure lateral mobility of membrane components in cell/substrate contact regions by fluorescence redistribution after pattern photobleaching (34).

The features of TIRF on cells lead to potential applications as follows. (*a*) TIRF greatly reduces fluorescence from cytoplasmically internalized label, cellular debris, and autofluorescence in thick cells, relative to fluorescence from membrane regions close to the substrate. This feature may allow

Figure 8 Cells in a mixed fibroblast/myoblast primary culture of embryonic rat muscle, labeled with the membrane soluble dye, 3,3'-dioctadecylindocarbocyanine. (*A*) TIRF on inverted microscope. (*B*) Same field in epi-illumination. (*C*) Same field in phase contrast. TIRF shows that the large round cell is making contact with the substrate only around its periphery and in one small region near its center. A 40X, 0.75 N.A., water immersion objective was used. Space bar = 50 μm.

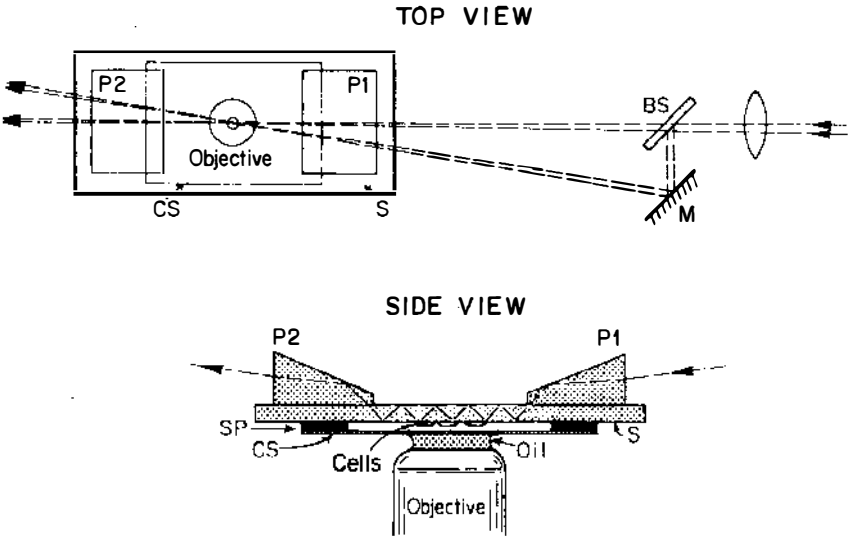

Figure 10 TIRF microscopy combined with interference fringes. The top view shows the two laser beams intersecting at the region under observation. The side view shows the path of a beam as it enters a prism P1, totally reflects multiple times in a glass slide to which cells are adhered (in this case on the lower surface), and exits via prism P2. Abbreviations are as follows: BS, beam splitter; CS, coverslip; L, lens; M, mirror; S, slide; SP, spacer.

detection of lower concentrations of fluorescence-marked membrane receptors than would otherwise be possible. (*b*) Study of the submembrane structure of the cell-substrate contact in thick cells can be facilitated. A fluorescently labeled cytoskeletal structure in the contact region can be visualized without interference from an out-of-focus background from fluorescently labeled cytoskeletal structure farther from the substrate. (*c*) By varying the incidence angle, the topography of the membrane facing the substrate can be mapped. (*d*) Reversibly bound fluorescent ligands on membrane receptors might be visualized without exciting background fluorescence from unbound ligand in the bulk solution. In this manner, certain cell surface receptors might be studied without the necessity of blocking them by irreversible antagonists.

EXPERIMENTAL SUGGESTIONS

In setting up a TIRF system, one may encounter a number of questions about design and materials. The following suggestions may be helpful.

1. The prism used to couple the light into the system and the (usually disposable) slide or coverslip in which the total reflection takes place need not be exactly matched in refractive index.

2. The prism and slide may be optically coupled with glycerin, cyclohexanol, or microscope immersion oil, among other liquids. Immersion oil has a higher index of refraction (thereby avoiding possible total internal reflection at the prism/glycerin interface for low incidence angles) but tends to be more autofluorescent (even the "extremely low" fluorescence types). This problem is usually not important to TIRF microscopy but can be serious in large area applications.
3. The prism and slide can both be made of ordinary optical glass for many applications, unless shorter penetration depths arising from higher refractive indices are desired. (More exotic high refractive index materials such as sapphire, titanium dioxide, and strontium titanate can yield penetration depths as low as $\lambda_0/20$.) However, optical glass does not transmit light below about 310 nm and also has a dim autoluminescence with a long (several hundred microsecond) decay time, which can be a problem in some photobleaching experiments. The autoluminescence of high quality fused silica (often called "quartz") is much lower.
4. The total internal reflection surface need not be polished to a higher degree than a standard commercial microscope slide.
5. Either a laser or conventional arc light source will suffice for study of macroscopic areas. But in TIRF microscopy, a conventional light source is difficult to focus to a small enough region at high enough intensity while still retaining sufficient collimation to avoid partial light transmission through the interface; a laser is more desirable here.
6. Illumination of surface-adsorbed proteins can lead to apparent photochemically-induced cross-linking and also to photobleaching at the higher range of intensities that might be used in TIRF studies. Apparent cross-linking, measured as a slow, continual, illumination-dependent increase in observed fluorescence, can be inhibited by 0.05 M cysteamine, among other substances; photobleaching can be reduced somewhat by deoxygenation or by 0.01 M sodium dithionite, among other substances.

ACKNOWLEDGMENTS

We thank Peter M. Torgerson of the University of California, San Francisco, and Adrienne Brian of Stanford University for permitting citation of some of their unpublished observations. This work was supported by USPHS NIH grant #14565 (to D.A.).

Literature Cited

1. Adam, G., Delbruck, M. 1968. In *Structural Chemistry and Molecular Biology*, ed. R. Alexander, D. Norman, pp. 198–215. San Francisco: Freeman
2. Aiginger, H., Wobrauschek, R. 1951. *J. Radioanal. Chem.* 61:281–93
3. Ambrose, E. J. 1961. *Exp. Cell Res. Suppl.* 8:54–73

4. Axelrod, D. 1981. *J. Cell Biol.* 89:141–45
5. Axelrod, D., Thompson, N. L., Burghardt, T. P. 1983. *J. Microsc.* 129:Pt. 1, pp. 19–28
6. Beissinger, R. L., Leonard, E. F. 1980. *Am. Soc. Artif. Internal Organs* 3:160–75
7. Born, M., Wolf, E. 1975. *Principles of Optics.* New York: Pergamon. 5th ed.
8. Burghardt, T. P. 1983. *J. Chem. Phys.* 78:5913–19
9. Burghardt, T. P. 1983. Submitted for publication
10. Burghardt, T. P., Axelrod, D. 1981. *Biophys. J.* 33:455–68
11. Burghardt, T. P., Axelrod, D. 1983. *Biochemistry* 22:979–85
12. Burghardt, T. P., Thompson, N. L. 1984. *Opt. Eng.* In press
13. Carniglia, C. K., Mandel, L., Drexgage, K. H. 1972. *J. Opt. Soc. Am.* 62:479–86
14. Chew, H., Wang, D., *Appl. Opt.* 18:2679–87
15. Eagen, C. F., Weber, W. H., McCarthy, S. L., Terhune, R. W. 1980. *Chem. Phys. Lett.* 75:274–77
16. Fringeli, U. P., Gunthard, Hs. H. 1981. In *Membrane Spectroscopy*, New York: Springer-Verlag
17. Haller, G. L., Rice, R. W., Wan, Z. C. 1976. *Catal. Rev. Sci. Eng.* 13:259–84
18. Harrick, N. J. 1967. *Internal Reflection Spectroscopy.* New York: Wiley Intersc.
19. Harrick, N. J., Loeb, G. I. 1973. *Anal. Chem.* 45:687–91
20. Harrick, N. J., Loeb, G. I. 1982. *Mod. Fluorescence Spectrosc.* 1:211–25
21. Hirschfeld, T. 1965. *Can. Spectrosc.* 10:128
22. Hirschfeld, T., Block, M. J. 1977. *Opt. Eng.* 16:406–7
23. Hirschfeld, T., Block, M. J., Mueller, W. 1977. *J. Histochem. Cytochem.* 25:719–23
24. Iwamoto, R., Miya, M., Onta, K. 1981. *J. Chem. Phys.* 74:4780–90
25. Kronick, M. N., Little, W. A. 1975. *J. Immunol. Methods* 8:235–40
26. Lee, E.-H., Benner, R. E., Fen, J. B., Chang, R. K. 1979. *Appl. Opt.* 18:862–68
27. Lok, B. K., Cheng, Y.-L., Robertson, C. R. 1983. *J. Colloid Interface Sci.* 91:87–102
28. Lok, B. K., Cheng, Y.-L., Robertson, C. R. 1983. *J. Colloid Interface Sci.* 91:104–16
29. McGuirk, M., Carniglia, C. K. 1977. *J. Opt. Soc. Am.* 67:103–7
30. Memming, R. 1974. *Faraday Discuss. Chem. Soc.* 58:261–70
31. Palik, E. D., Holm, R. T. 1978. *Opt. Eng.* 17:512–24
32. Rabolt, J. F., Santo, R., Swalen, J. D. 1979. *Appl. Spectrosc.* 33:549–51
32a. Rockhold, S. A., Quinn, R. D., Van Wagenen, R. A., Andrade, J. D., Reichert, M. 1983. *J. Electroanal. Chem.* 150:261–75
33. Selser, J. C., Rothschild, K. J., Swalen, J. D., 48:1690–93
34. Smith, B. A., McConnell, H. M. 1978. *Proc. Natl. Acad. Sci. USA* 75:2759–63
35. Thompson, N. L. 1982. *Biophys. J.* 38:327–29
36. Thompson, N. L., Axelrod, D. 1983. *Biophys. J.* 43:103–14
37. Thompson, N. L., Burghardt, T. P. 1983. Submitted for publication
38. Thompson, N. L., Burghardt, T. P., Axelrod, D. 1981. *Biophys. J.* 33:435–54
39. Tweet, A. G., Gaines, G. L., Bellamy, W. D. 1964. *J. Chem. Phys.* 40:2596–2600
40. Van Wagenen, R. A., Rockhold, S., Andrade, J. D. 1982. In *Biomaterials: Interfacial Phenomena and Applications, Adv. Chem.*, Peppas, 199:351–70
41. Watkins, R. W., Robertson, C. R. 1977. *J. Biomed. Mater. Res.* 11:915–38
42. Weber, W. H., Eagen, C. F. 1979. *Opt. Lett.* 4:236–38
43. Weis, R. M., Balakrishnan, K., Smith, B. A., McConnell, H. M. 1982. *J. Biol. Chem.* 257:6440–45
44. Wood, R. W. 1934. *Physical Optics*, pp. 419–20. New York: Macmillan. 3rd ed.